NDT&E International 116 (2020) 102339

Contents lists available at ScienceDirect

NDT and E International

journal homepage: http://www.elsevier.com/locate/ndteint

Evaluation of subsurface defects in metallic structures using laser ultrasonic technique and genetic algorithm-back propagation neural network

Kaixing Zhang [a,f,1], Gaolong Lv [a,b,c,1], Shifeng Guo [b,c,d,*], Dan Chen [b,c], Yanjun Liu [e,**], Wei Feng [b,c,d]

[a] College of Mechanical and Electronic Engineering, Shandong Agricultural University, Tai'an, 271018, China
[b] Shenzhen Key Laboratory of Smart Sensing and Intelligent Systems, Shenzhen Institute of Advanced Technology, Chinese Academy of Sciences, Shenzhen, 518055, China
[c] Guangdong Provincial Key Lab of Robotics and Intelligent System, Shenzhen Institute of Advanced Technology, Chinese Academy of Sciences, Shenzhen, 518055, China
[d] CAS Key Laboratory of Human-Machine Intelligence-Synergy Systems, Shenzhen Institute of Advanced Technology, Chinese Academy of Sciences, Shenzhen, 518055, China
[e] Department of Electrical and Electronic Engineering, Southern University of Science and Technology, Shenzhen, 518055, China
[f] Shandong Agricultural Equipment Intelligent Engineering Laboratory, Tai'an, 271018, China

ARTICLE INFO

Keywords:
Laser ultrasonics
Machine learning
Neural network
Subsurface defect
NDE
Rayleigh ultrasonic wave

ABSTRACT

An effective nondestructive evaluation technique that enables the detection and quantification of subsurface defects is highly demanded for assuring safety and reliability of safety-critical structures. In this work, an improved genetic algorithm-back propagation neural network (GA-BPNN) model and non-contact laser ultrasonic technique are combined to quantify the width of subsurface defects. An experimentally validated numerical model that simulates the interaction of laser-generated Rayleigh ultrasonic waves with subsurface defects is firstly established, which is further utilized to generate a large number of labeled laser ultrasonic signals for training the GA-BPNN model. A total number of 189 data are obtained from simulation and experiments, with 173 simulated signals for training the GA-BPNN model and the remaining 13 simulated signals together with 3 experimental signals for verifying the performance of the trained GA-BPNN model. Five features including three time-domain features (maximum, minimum and peak-to-peak value of the Rayleigh ultrasonic waves) and two frequency-domain features (F_c, BW_{-6dB}), which are identified sensitive to the width of subsurface defects by both experiments and simulation, are extracted as inputs to train the machine learning algorithm. The result demonstrates that the GA-BPNN model trained with the combination of time and frequency features has the average error of 2.15%, which is substantially smaller than the errors obtained from the model trained with only time-domain features and frequency-domain features, with the average errors of 4.43% and 21.81%, respectively. This work proves the feasibility and reliability to quantify the width of subsurface defects in metallic structures using laser ultrasonic technique and the improved GA-BPNN algorithm.

1. Introduction

The subsurface defects that near but not exposed at the surface of structures will gradually grow into a series of large defects unnoticed, and may ultimately cause catastrophic accidents if not detected in advance [1,2]. Therefore, an effective nondestructive evaluation (NDE) technique that enables the detection and quantification of subsurface defects is crucial and highly demanded for assuring safety and reliability of safety-critical structures. Ultrasonic inspection is a well-established technique for identifying and evaluating internal defects of structures of various materials [3–5], such as multilayered bonded composites, friction stir welded joints [6–8]. However, the conventional ultrasonic NDE techniques are mostly contact based and require additional coupling and fixtures for generation and detection of ultrasonic signals

* Corresponding author. Shenzhen Key Laboratory of Smart Sensing and Intelligent Systems, Shenzhen Institute of Advanced Technology, Chinese Academy of Sciences, Shenzhen, 518055, China.
** Corresponding author.
E-mail addresses: sf.guo@siat.ac.cn (S. Guo), yjliu@sustech.edu.cn (Y. Liu).
[1] The authors contributed equally to this work.

https://doi.org/10.1016/j.ndteint.2020.102339
Received 7 January 2020; Received in revised form 14 July 2020; Accepted 25 July 2020
Available online 12 August 2020
0963-8695/

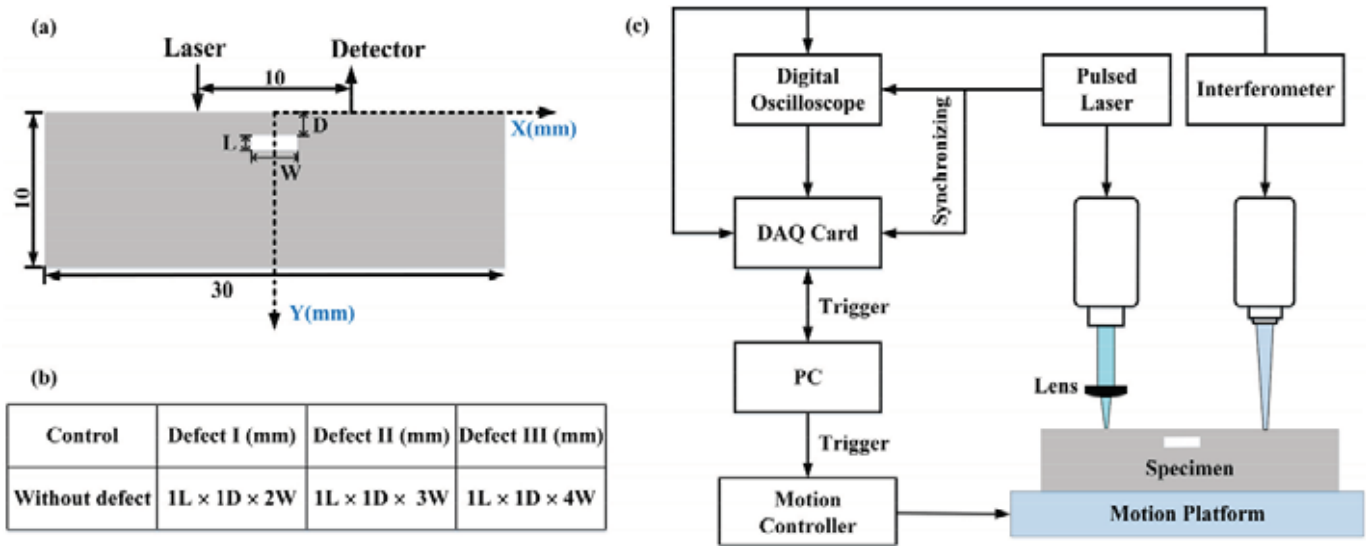

Control	Defect I (mm)	Defect II (mm)	Defect III (mm)
Without defect	1L × 1D × 2W	1L × 1D × 3W	1L × 1D × 4W

Fig. 1. (a) The dimension of the Al alloy specimen and experimental condition. (b) The defect types and defect dimensions. L, D and W are abbreviations of defect height, defect depth to surface, and defect width, respectively. (c) The schematic of the experimental setup for evaluating crack width with ultrasonic waves excited by pulsed laser and detected by a laser interferometer.

[9], which is not feasible in harsh environment. The pulsed laser generated ultrasound (laser ultrasonics) is considered as a promising approach in ultrasonic NDE because of its advantages in non-contact generation and detection [10]. Unlike the piezoelectric ultrasonic technique with contact based measurement, the laser ultrasonic technique, with ultrasonic waves generated and detected by lasers, is purely a non-contact detection method. Therefore its detection performance is not affected by the environment factors, such as high temperature, heavy electromagnetic interference, etc. [11,12], and enables accessibility to limited and complicated structures [13–15].

The laser ultrasonics, using a pulsed laser to generate ultrasonic waves and adopting a wide band laser coupled to an interferometer to measure the surface displacements of solids, has been implemented for inspecting structural materials with various defects. Liu et al. [16] investigated a free contact dual laser ultrasonic system to detect fatigue crack using a nonlinear ultrasonic modulation technique. Valle et al. [17] analyzed the length and location of surface-breaking defect with varied branched geometries by investigating the behavior of far-field reflection and near-field enhancement with cracks. Guo et al. [18] studied micro-defects detection on aluminum plates using Raleigh waves generated by laser. Zhang et al. [11] used the pulsed laser generated guided waves to characterize disbonded joints in a bonded composite. The above-mentioned work involves establishing the linear relationship between defect sizes and the parameters of the received ultrasonic signals, and estimates the defect sizes by comparing the ultrasonic signals with that from non-defect samples. However, in most cases, the correlation between defect sizes and ultrasonic signal is not linearly correlated and it is expensive and time-consuming to obtain such correlation experimentally. The emerging advances in simulation enables mitigating the labor operation and time consumption of acquisition a large number of labeled samples from experiment. Meanwhile, the detection accuracy and efficiency can be improved to a great extent by means of machine learning algorithm when a large number of labeled samples from experimentally validated numerical simulation are available.

The machine learning methods such as artificial neural networks solve complex problems by constructing computational models that mimic the human brain. In recent years, neural networks have been widely implemented in the NDE area and extensive research has been conducted for defects identification [19,20]. Yang et al. [21] proposed a method to evaluate the depth and orientation of initial defect in the turbine discs combining artificial neural networks (ANN) and phased array ultrasonic transducer technique. Deng et al. used kernel-based principal component analysis (KPCA) algorithm and extreme learning machine (ELM) to extract the defect parameters of the eddy current signals to identify and classify cracks [22]. Kesharaju et al. [23] established an on-line quality detection system based on feed-forward neural network and ultrasonic sensing technique to detect, locate and classify various manufacturing cracks. The above work demonstrated that machine learning algorithms (such as neural networks) have been well implemented for various NDE application. The neural network algorithm has also been reported in the laser ultrasonic applications. Chen et al. [24] applied pulsed laser and piezoelectric probe to generate and receive ultrasound, and combined improved BP neural network to detect different types of cracks. Bagheri et al. [25] combined the hybrid laser-immersion transducers system and unsupervised neural network for the classification of defects type. Chen et al. [26] proposed the combination of machine learning algorithms and processed plasma emission spectra to detect and classify defects. However, the above work mainly utilized the machine learning algorithms (such as support vector machine, SVM) and laser ultrasonics for the classification of defects type, not to quantitatively evaluate the size of defects. Li et al. [27] recently reported a study by using numerically simulated scanning laser source data and machine learning to identify and quantify surface breaking cracks. However, this work investigates the surface cracks, which is more accessible compared with subsurface defects. In addition, it is a pure simulation work and the established numerical model is without experimental verification, which substantially affects the feasibility of the machine learning classifier trained by the labeled samples from numerical simulation. To evaluate the subsurface defects using non-contact laser ultrasonic technique and machine learning method, the validated numerical model and reliable machine learning algorithms with sensitive features reflecting the defects are highly demanded.

In this work, an effective nondestructive evaluation technique that enables the quantification of subsurface defects of metallic structure is developed by the combination of the improved genetic algorithm-back propagation neural network (GA-BPNN) model and non-contact laser ultrasonic technique. The subsurface defect is defined as the defect with depth within one wavelength of laser generated Rayleigh ultrasonic waves. The experimentally validated numerical model that is based on the finite element method (FEM) is firstly established to simulate the

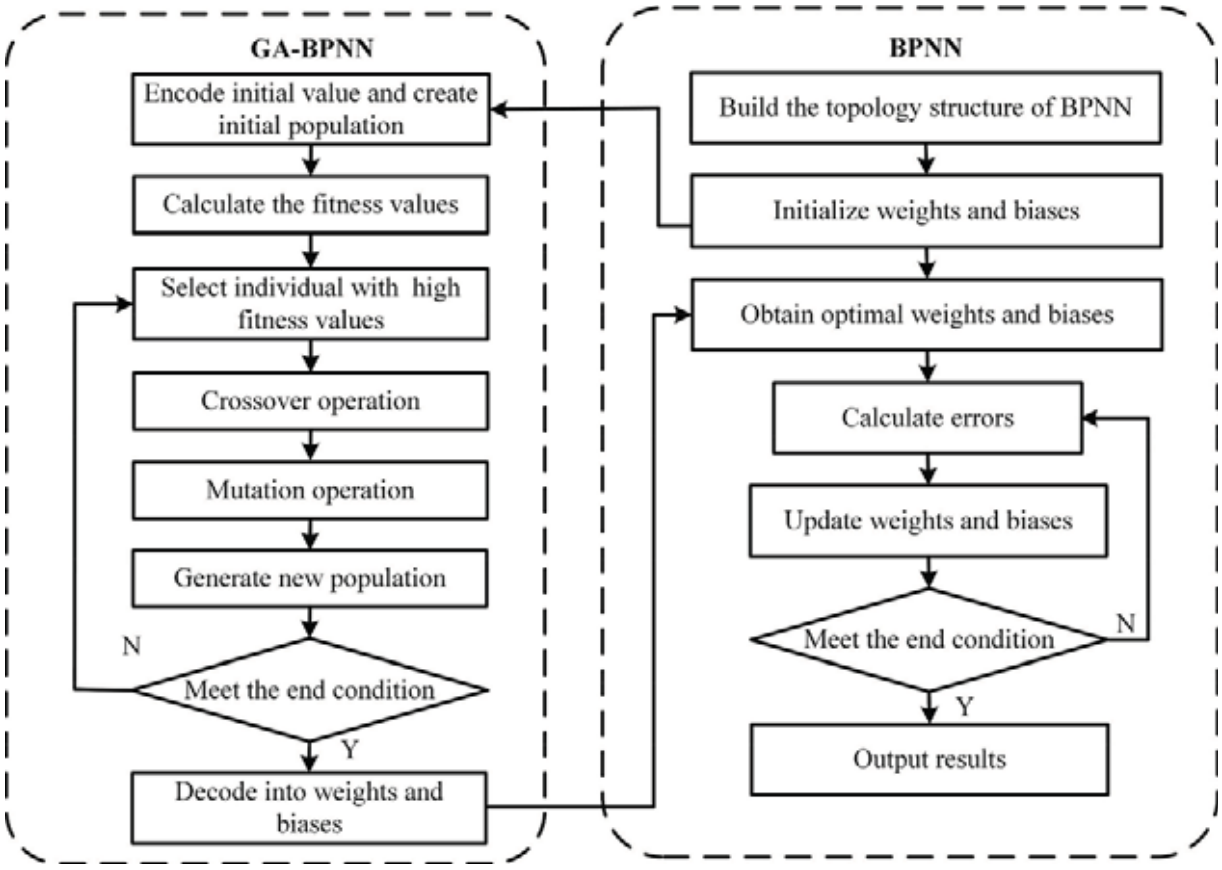

Fig. 2. The flow chart of BPNN model with genetic algorithm.

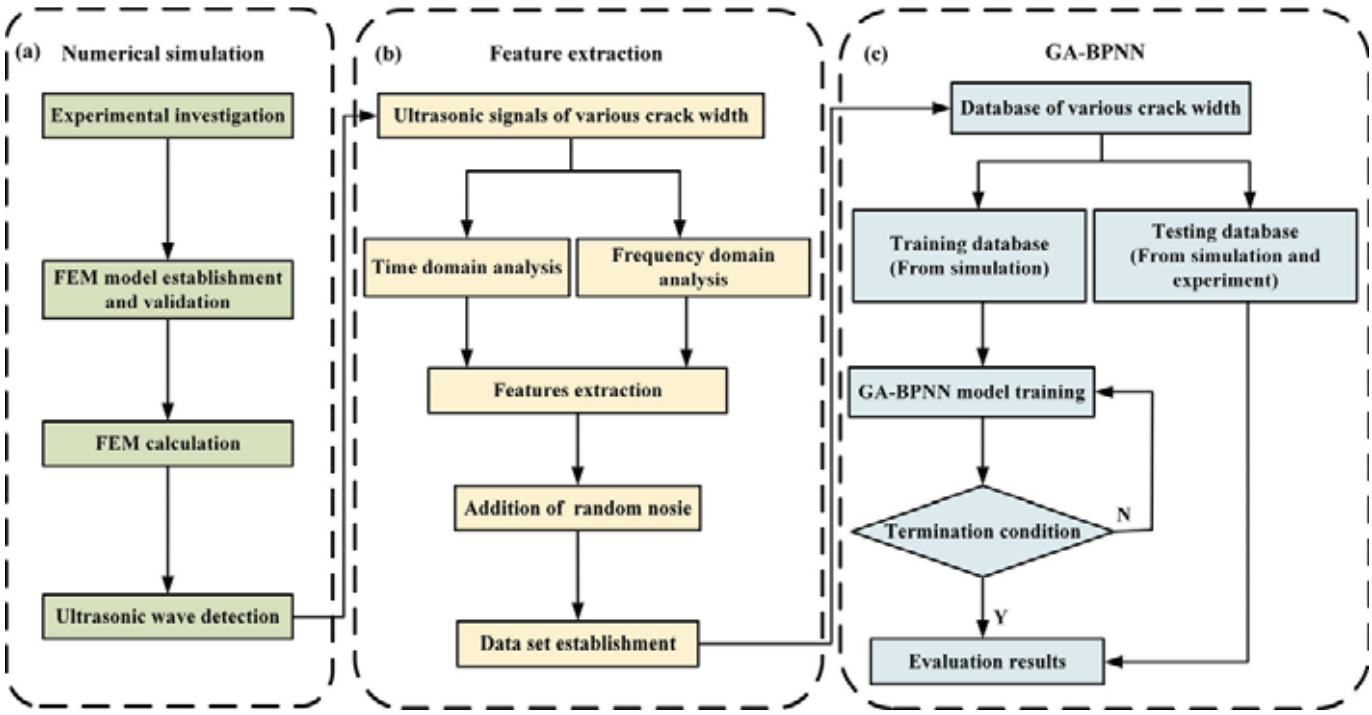

Fig. 3. The flow chart of the combination of the GA-BPNN model and laser ultrasonic technique for evaluating the width of subsurface cracks. (a) Numerical simulation. (b) Feature extraction. (c) GA-BPNN model evaluation.

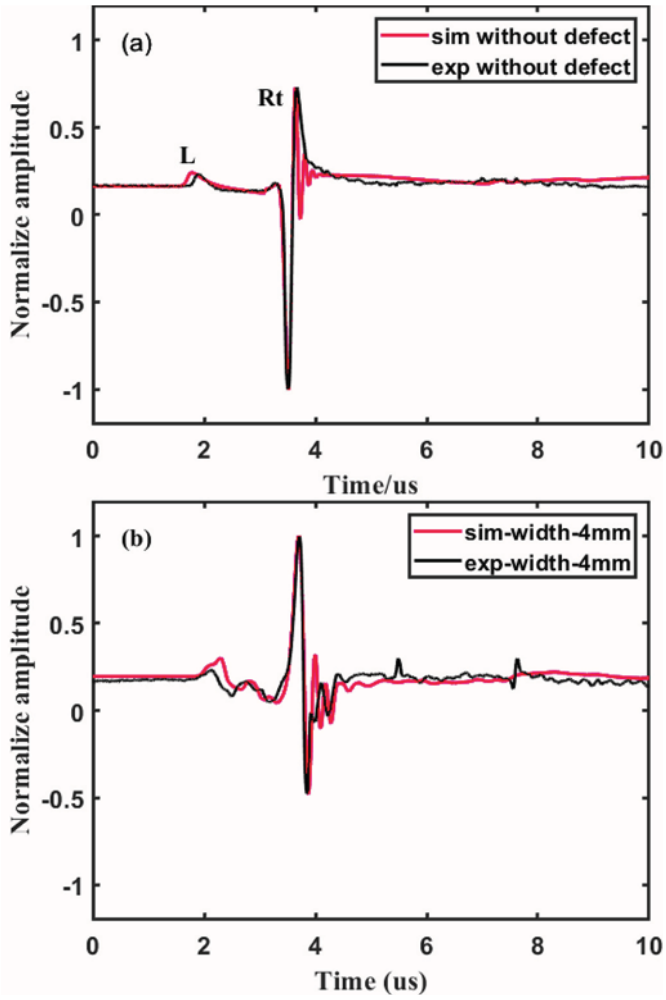

Fig. 4. The comparison between experimental and simulation results. (a) Without crack. (b) Crack width of 4 mm.

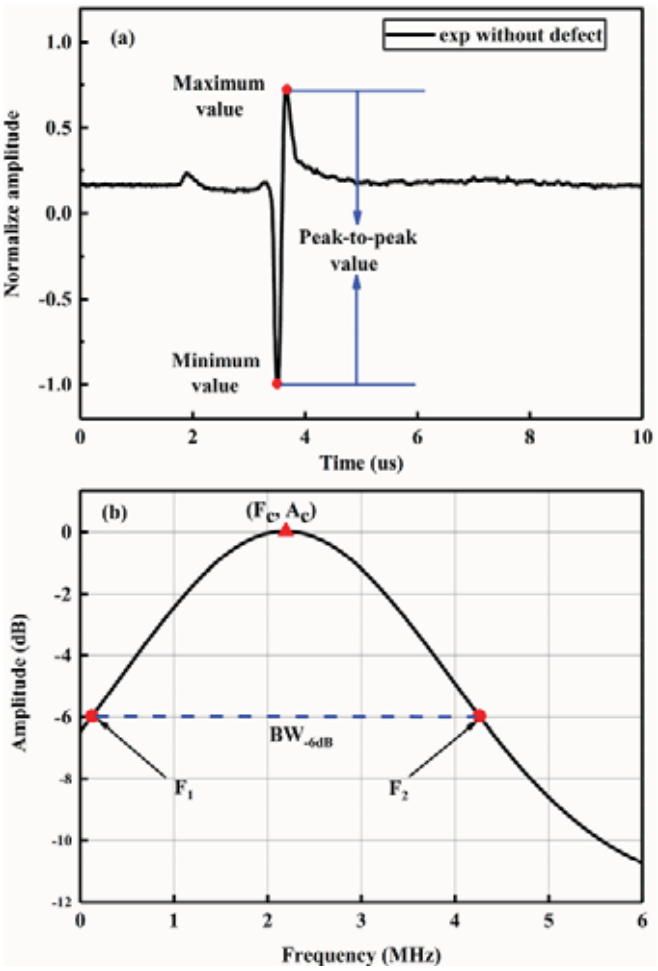

Fig. 6. Feature selection for training the GA-BPNN model. (a) Features of time domain (Maximum, Minimum, and Peak-to-peak value). (b) Features from frequency domain (Fc and BW_{-6dB}).

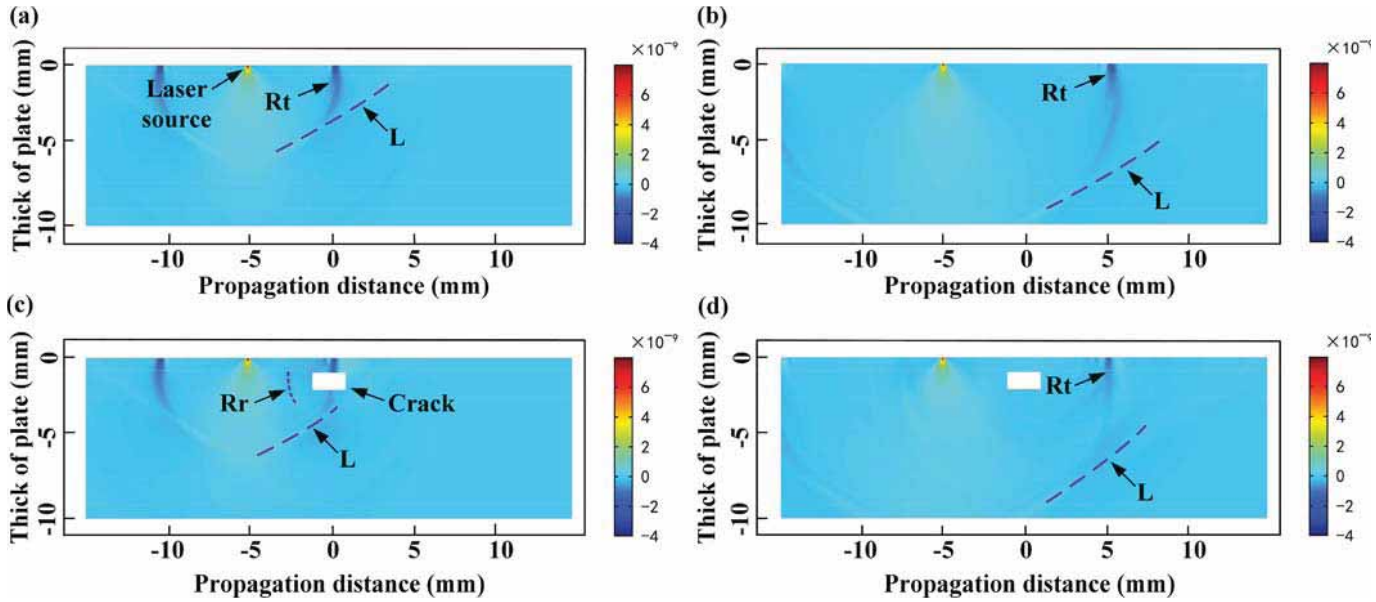

Fig. 5. Simulation results of laser generated ultrasonic waves propagation in the specimen without and with subsurface defects. (a) Wave detection at propagation distance of 5 mm (without crack). (b) Wave detection at propagation distance of 10 mm (without crack). (c) Wave detection at propagation distance of 5 mm (2 mm crack width). (d) Wave detection at propagation distance of 10 mm (2 mm crack width).

Table 1
Material properties of Al alloy for numerical simulation.

Density ρ(kg/m^3)	Young's Modulus E(GPa)	Poisson's ratio υ	Thermal expansion α(μK)	Thermal conductivity k(Wk/m)	Heat capacity C_v(JK/kg)	Reflection coefficient R
2780	71	0.33	23	120	880	0.9

Table 2
The configuration parameters of the GA-BPNN model.

Parameters	Value
Learning rate	0.015
Training goal	0.001
Epoch	1000
Training function	trainlm
Transfer function	sigmoid
Cycle index	10000
Maxgen	60
Selectivity factor	1.0
Crossover factor	0.3
Mutation factor	0.1
Population size	40

Table 3
The average prediction errors with different features.

Features	Time domain	Frequency domain	Time and frequency domain
Average error	4.43%	21.81%	2.15%

interaction of laser-generated Rayleigh ultrasonic waves with subsurface defects, which is further used to produce sufficient reliable laser ultrasonic signals for training and verifying the GA-BPNN model. The characteristics of the laser generated Rayleigh waves, identified by both experiments and simulation, which are highly dependent on the width of subsurface cracks, are extracted as input features for training the machine learning model. The time and frequency domain features of the simulated Rayleigh waves are combined to train the genetic algorithm-back propagation neural network (GA-BPNN), which is further validated and tested with a set of hybrid signals from both experiments and simulation to predict the width of subsurface cracks. The rest of the paper is organized as follows: Section 2 describes the laser ultrasonic method for evaluating the widths of subsurface defects, including the experimental and numerical details of laser ultrasound method, and the improved GA-BPNN machine learning algorithm; Section 3 illustrates and discusses the results of the prediction accuracy of defects width using the combination of numerical model and GA-BPNN algorithm; Section 4 concludes this work.

2. Materials and methods

2.1. Specimen and experimental details

The aluminum (Al) alloy (2024) plates with various subsurface crack widths were designed and fabricated for investigation the correlation between laser ultrasonic signals and defect sizes. Four subsurface defects with various widths of 0, 2, 3, and 4 mm were fabricated using electrical discharge machining (EDM) and wire cutting method. Each sample contains only one artificial crack. The schematic and dimensions of the specimens and defects are shown in Fig. 1(a and b), and the relatively large dimension of the plate is to exclude the reflected signals from boundaries. The schematic of the experimental setup is shown in Fig. 1 (c). A Nd:YAG pulsed laser (Centurion+) with the wavelength of 1064 nm, pulse duration of 12 ns, and pulse energy of 0–50 mJ is used, which

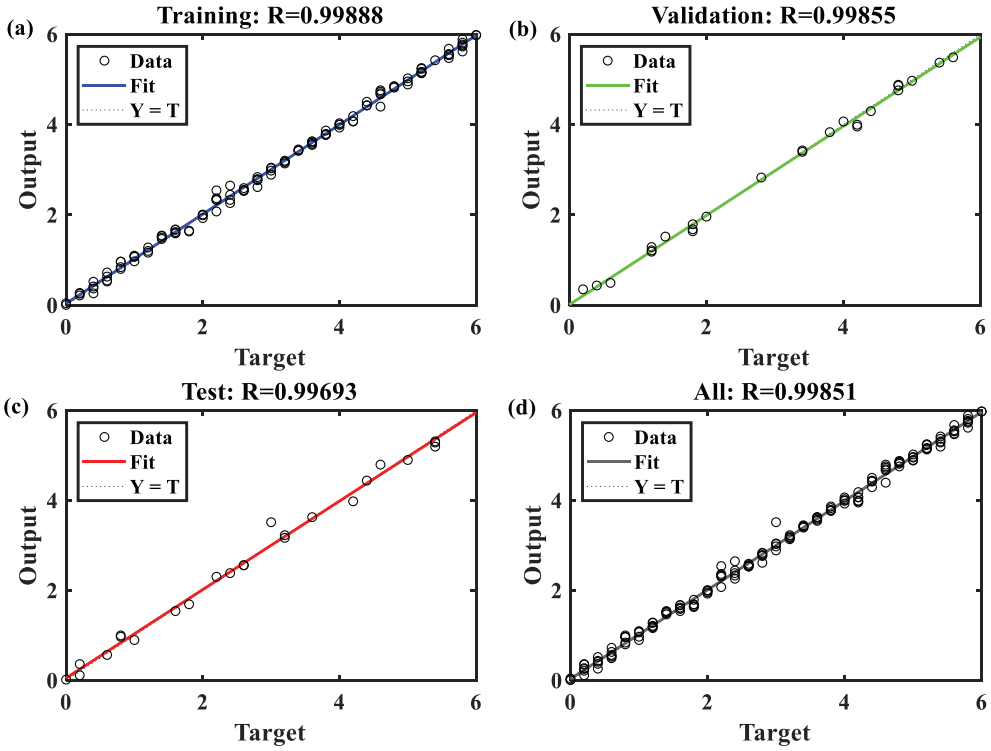

Fig. 7. ANN coefficient relation. (a) Training. (b) Validation. (c) Test. (d) All value.

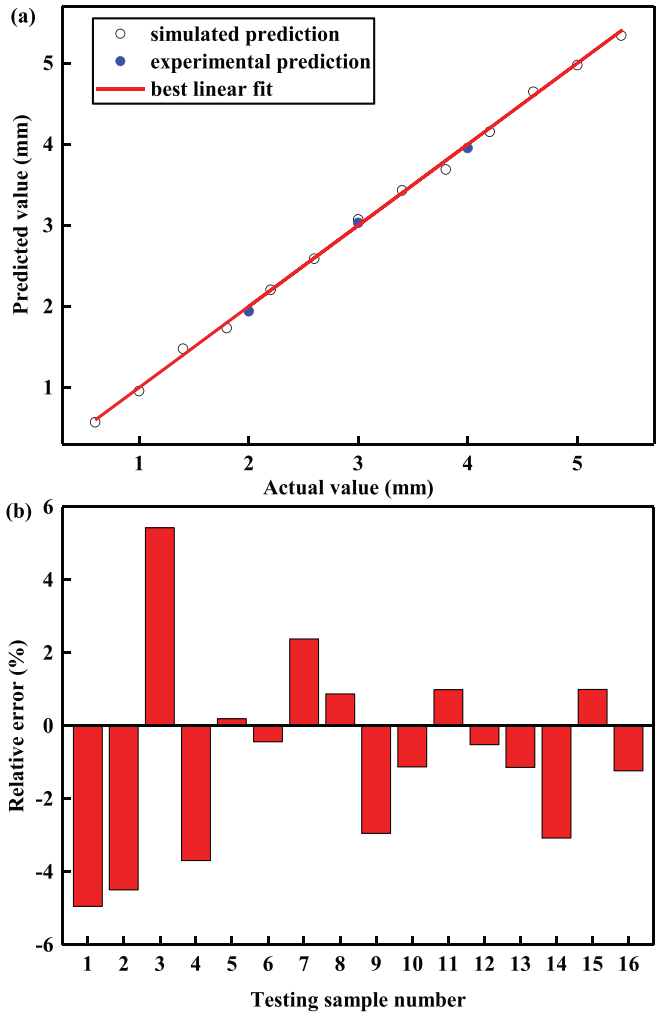

Fig. 8. (a) Comparison of actual value and predicted value. (b) Relative error of the actual value and predicted value.

can generate Rayleigh ultrasonic waves with −6 dB bandwidth of 4 MHz and central frequency of 2.2 MHz (Fig. 6(b)). A laser interferometer (TEMPO) is applied to acquire the out-of-plane displacement of the ultrasonic waves, using an adaptive reference beam and two-wave mixing in a photorefractive crystal. The pulsed laser beam is shifted and focused on the specimen plate surface by manipulating the cylindrical mirror and convex lens. The laser source is fixed at −5 mm from the center of sub-surface defects in the X direction and the detector is positioned at +5 mm from the center of the defect to detect the transmitted Rayleigh waves [Fig. 1 (a)]. The acquired signals are digitalized by a high-resolution data acquisition card (DAC) with sampling frequency of 250 MHz, trigged by the NI PXI device, transmitted to a computer to generate ultrasonic time-domain signals, and averaged over 128 times to improve the signal-noise ratio. To exclude any effect from surface roughness, the surface roughness of the specimens is maintained at about 0.8 μm. The specimens are fixed on the table during laser ultrasonic experiments and same boundary condition is implemented for numerical simulation model.

2.2. Theory and numerical model

2.2.1. Laser ultrasound generation based on thermoelastic mechanism

As the pulsed laser irradiates on the surfaces of Al alloy plates, part of the energy is absorbed and generates a transient temperature field. The non-uniform temperature distribution drives the thermal expansion and thermal stresses to generate stress waves. In the thermoelastic mechanism, the laser-induced ultrasonic waves can be described as a thermal transfer formula and thermoelastic displacement formula:

$$\rho C_v \frac{\partial T}{\partial t} - k\nabla^2 T = Q \tag{1}$$

$$\alpha(3\lambda + 2\mu)\nabla T + \mu\nabla^2 \mathbf{u} + \rho\frac{\partial^2 \mathbf{u}}{\partial t^2} = (\lambda + 2\mu)\nabla(\nabla \cdot \mathbf{u}) \tag{2}$$

where T is the temperature field in metal material, k represents the thermal conductive coefficient, C_v denotes the thermal capacity, λ and μ are the Lame constants, $\mathbf{u}$ is the time-dependent displacement vector, ρ and α are the density and thermal expansion factor, respectively. The heat source Q can be described as:

$$Q = I_0(1 - R)f(x)g(t) \tag{3}$$

where I_0 is the power density of the incident laser, R represents the reflection coefficient of the material surface. $g(t)$ and $f(x)$ are the temporal and spatial distributions of the laser pulse, respectively, which can be expressed as:

$$f(x) = \exp\left(-\frac{x^2}{x_0^2}\right) \tag{4}$$

$$g(t) = \frac{t}{\tau}\exp\left(-\pi\frac{t}{\tau}\right) \tag{5}$$

where x_0 is laser spot radius, τ is the rise time of the pulsed laser. The temperature field and displacement field initial conditions can be expressed as:

$$\dot{T}(x, y, t)|_{t=0} = 0, \quad T(x, y, t)|_{t=0} = 300K \tag{6}$$

$$\dot{\mathbf{u}}(x, y, t)|_{t=0} = \mathbf{u}(x, y, t)|_{t=0} = 0 \tag{7}$$

For most metallic materials, the boundary condition at the irradiated region $z = 0$ is written as

$$\mathbf{n}[\sigma - (3\lambda + 2\mu)\alpha\nabla T \cdot \mathbf{I}] = 0 \tag{8}$$

where $\mathbf{n}$ is the normal unit vector of the material surface, σ is the stress tensor, and $\mathbf{I}$ is the unit tensor.

2.2.2. Numeric simulation

According to equations (1) and (2), the thermodynamic equations can be described as:

$$[\mathbf{K_T}]\{\dot{\mathbf{T}}\} + [\mathbf{K}]\{\mathbf{T}\} = \{\mathbf{P_1}\} + \{\mathbf{P_2}\} \tag{9}$$

Where $[\mathbf{K_T}]$ is the conductivity matrix, $\{\mathbf{T}\}$ is the temperature vector, $\{\mathbf{P_1}\}$ is the heat flux vector, $\{\mathbf{P_2}\}$is the heat source vector, $[\mathbf{K}]$ is the heat capacity and $\{\dot{\mathbf{T}}\}$ is the temperature rise rate vector.

For ultrasonic waves propagation, the damping is neglected and the finite element formula can be defined as:

$$[\mathbf{K}]\{\mathbf{U}\} + [\mathbf{M}]\{\ddot{\mathbf{U}}\} = \{\mathbf{F_{ext}}\} \tag{10}$$

where $[\mathbf{K}]$ and $[\mathbf{M}]$ are the stiffness matrix and mass matrix, $\{\mathbf{U}\}$ and $\{\ddot{\mathbf{U}}\}$ are the displacement vector and acceleration vector, and $\{\mathbf{F_{ext}}\}$ is the external force vector that can be represented as:

$$\int_{Ve} [\mathrm{B}]^{\mathrm{T}}[\mathrm{E}]\{\varepsilon_0\}\mathrm{dV} \tag{11}$$

where $[\mathbf{E}]$ is the matrix of material parameters, $\{\boldsymbol{\varepsilon_0}\}$ is the thermal strain vector, and $[\mathbf{B}]^{\mathrm{T}}$ is the transpose of the shape function matrix. The specified calculation procedure of FEM can be acquired in the literature [8,28].

The numerical model is established using a commercial finite

element software Comsol Multiphysics to simulate the generation and detection of laser ultrasonic waves on Al alloy plates, with artificial subsurface cracks of various dimensions. The rectangle subsurface cracks are modeled with fixed height and depth of 1 mm, and width varied from 0 to 6 mm in the X direction with step size of 0.2 mm, shown in Fig. 1 (a). The laser source is fixed at −5 mm from the center of the sub-surface defect in the X direction and the detector is positioned at +5 mm from the center of the defect [Fig. 1(a)]. All the parameters with regards to the laser power density, rise time, pulse duration are set the same as experimental conditions. The material properties of the Al alloy for simulation are listed in Table 1.

As the convergence of simulation solution is substantially affected by the temporal and spatial resolution of the proposed model. The accuracy and computing time are decided by the iteration time step of the numerical simulation and a proper time step (Δt) of the numerical simulation can be determined [20].

$$\Delta t = \frac{1}{20 f_{\max}} \tag{12}$$

where $f_{\max}$ is the highest frequency of the ultrasound. As the element type is crucial to determine the fidelity of numerical simulation, the quadrilateral elements with four nodes are applied. Generally, the mesh size is more than 10 nodes in a wavelength [29].

$$L_e = \frac{\lambda_{\min}}{10} \tag{13}$$

where $\lambda_{\min}$ is the shortest wavelength of laser-generated ultrasound and L_e is the mesh size.

Therefore, the time step is set to 4 ns and the mesh size near the laser irradiation area is set to 2 μm, while the maximum size of elements away from the heated-affected area is set to 20 μm, which can meet the change of temperature gradient, meanwhile save computation time and guarantee the continuous spread of ultrasound. The low-reflecting boundary condition is applied on both sides of the model to suppress the reflection of ultrasound waves. The numerical simulation time is set to 10 μs, which is enough to detect the transmitted waves. In our model, the node displacement at the detection location is extracted for the acquisition of ultrasonic signal, and no additional sensor model is therefore needed. To predict the width of different defects, thirty-one cases were generated with the widths of subsurface defects range from 0 to 6 mm, with an increment of 0.2 mm.

2.3. GA-BPNN evaluation technique

The artificial neural network (ANN) is an artificial intelligence method that mimics the operation and computational performance of human brains, which can reflect the latent linear or nonlinear relationships between input and output data [30]. ANN can obtain information by training vast amount of data. The most commonly used algorithm for training the ANN is back propagation neural network (BPNN) [31], which is a supervised learning method for dealing with a complex system and nonlinear problem, firstly presented by Rumelhart [32]. Although BPNN has good predictive performance, some drawbacks such as over-fitting, local minima and longer training time still exists [33,34]. In order to improve its performance, the genetic algorithm with global stochastic search capacity is applied to optimize the original biases and weights of BPNN to avoid local convergence and obtain accurate solutions [35,36]. The global optimum solution is acquired by genetic algorithm, and Fig. 2 shows the flow chart for optimizing BPNN model with genetic algorithm. As an evolutionary optimization technique, genetic algorithm starts with initial population (initial solution), develops toward the global optimal solution, and stops searching when the stopping condition is satisfied [37]. The quality of the global optimal solution relies highly on the preliminary solution fed to the GA-BPNN model. In the case of random evolution (in Fig. 2), a series of stochastic individuals are taken as the initial solution (initial population), which can be deciphered to biases and weights [38,39]. The mean absolute percentage error (MAPE) [19] is selected as fitness function to calculate the fitness values of all individuals.

$$MAPE = \frac{1}{k}\sum_{j=1}^{j=k}\frac{|E_j - P_j|}{E_j} \tag{14}$$

Where k is the total number of network output nodes, E_j and P_j are the expected value and predicted value of the j-*th* node, respectively. The excellent with high fitness value can be obtained from the initial population through select, crossover and mutation operation. Individuals with better adaptability (high fitness value) are retained, the population evolves repeatedly, and the global optimal solution is obtained finally. After meeting the termination condition (goal value or the maximum number of executions), the optimal solution is decoded to the optimal weights and biases, and the neural network model is trained to achieve goal value. The complementary advantages can be achieved after combining the genetic algorithm with the BPNN.

The performance of the GA-BPNN model for estimating the width of the subsurface crack can be appraised by using the following statistical indicators [40–42]: (i) Mean Absolute Error (*MAE*); (ii) Willmott's Index of Agreement (*WI*); (iii) Root Mean Square Error (*RMSE*); (iv) Coefficient of Determination (R^2). The range of MAE and RMSE is between 0 and 1, and smaller values indicate better evaluation performance of the network model, and vice versa [43,44]. The range of R^2 and WI is between 0 and 1, and the larger values indicate better reliability of the fit model [45].

Fig. 3 shows the flow chart of the combination of the GA-BPNN model and laser ultrasonic technique for evaluation the width of subsurface cracks. The numerical simulation model is firstly established and experimentally validated for training the neural network model [Fig. 3 (a)]. The sensitive features in time and frequency domain of the Rayleigh ultrasonic waves are identified from experiments, and are extracted to represent the linear or non-linear relationship between the detected ultrasonic signal and various defect widths [Fig. 3(b)]. The GA-BPNN model is utilized to evaluate the crack width by using the established data set [Fig. 3(c)].

3. Results and discussion

3.1. Experimental results and numerical model validation

In this work, the interaction of laser-generated ultrasonic waves with various subsurface defects (crack width of 0, 2, 3 and 4 mm) is experimentally explored. Fig. 4 shows the representative time trace of the laser-generated ultrasonic waves, where L denotes the surface-skimming longitudinal wave identified by the measured velocity of 6100 m/s and Rt indicates transmitted Rayleigh ultrasonic waves, identified by the measured velocity of 3100 m/s. The experimental results show that Rayleigh ultrasonic waves are much stronger and more sensitive with the width of subsurface cracks compared with the longitudinal waves (by comparing the experimental ultrasonic signals from specimen with crack width of 0, 2, 3, 4 mm). It is therefore the Rayleigh ultrasonic wave is selected for training the neutral network and crack width evaluation in subsequent study.

To achieve reliable results, a significant amount of data is required for training the GA-BPNN model. However, it is extremely expensive and time consuming to acquire the training data from experiments. Therefore, a reliable and validated numerical model should be established to obtain enough data for training the neural network model. In this work, the simulations were conducted with the same parameters as experiments. The simulated and experimental data are normalized for comparison and the results show that the signals from simulation and experiment (from specimen with and without cracks) are in good agreement, with only very small fluctuations (Fig. 4). It therefore

suggests that the simulation model established is validated and it is reliable to use this simulation model to substitute experiments to obtain sufficient training data.

The propagation of the laser generated ultrasonic waves on the Al alloy plates is simulated, and both longitudinal waves (L) and Rayleigh ultrasonic waves (Rt) are observed (Fig. 5). For specimen without defects, the Rayleigh ultrasonic waves show no significant differences between two propagation distances, and no reflected waves are observed [Fig. 5(a)–(b)]. For specimen with subsurface cracks, the reflected Rayleigh ultrasonic wave (Rr) from cracks appear [Fig. 5 (c)–(d)]. A considerable part of the wave energy is reflected away by the crack resulting in significant attenuation in the transmitted Rayleigh ultrasonic wave compared with the intact specimen [Fig. 5(b)–(d)]. The variation in amplitudes of ultrasonic signals indicates that the Rayleigh ultrasonic waves contain the crack width information.

3.2. Feature extraction

Feature selection and extraction play essential role in training the neural network model. The most sensitive features relating to the width of subsurface cracks should be extracted from the transmitted Rayleigh ultrasonic waves to train the GA-BPNN model for automated crack detection and dimension evaluation. The experimental and simulation results (Fig. 3) show that the maximum, minimum and peak-to-peak value of the Rayleigh waves are substantially affected by the width of the subsurface cracks and are therefore selected as the sensitive features, shown in Fig. 6(a). The corresponding frequency spectrum is shown in Fig. 6(b). F_1 and F_2 are the lower and upper frequency corresponding to half of maximum amplitude, and the BW_{-6dB} (obtained by F_2–F_1) is selected as one frequency domain feature. The central frequency F_c calculated by $F_c = (F_1+F_2)/2$ is adopted as the other frequency domain feature. Therefore, five features are selected for training the GA-BPNN model, including three time-domain features (maximum, minimum, peak-to-peak value) and two frequency-domain features (F_c and BW_{-6dB}). To ensure the accuracy and robustness of the neural network, 5 varying levels of Gaussian random noise (1%, 2%, 3%, 4%, 5% relative to the original data) are added into the features, respectively, for expanding the data sets.

3.3. GA-BPNN training and testing

The trial and error method is implemented to determine the optimum structure of the machine learning model, which can reduce overfitting to a great extent. According to the optimum structure of GA-BPNN model in this study is determined as 5-11-1 (5 neurons in the input layer, 11 neurons in the hidden layer and one neuron in the output layer) and Table 2 shows the parameters of the GA-BPNN model for prediction the width of subsurface cracks.

A total number of 189 data are obtained from both simulation and experiments. The simulated data are comprised of 31 sets with crack width varying from 0 to 6 mm in steps of 0.2 mm, and each set is comprised of original data and contaminated data with 5 varying levels of Gaussian random noise. The experimental data are comprised of 3 sets with crack width of 2, 3 and 4 mm. The dataset with five features are set as the inputs and one parameter (the width of cracks) is set as the output of the GA-BPNN model. The 186 simulated data are randomly separated into 173 training data for training the neural network to obtain the optimized weights and biases, and the remaining 13 simulation data and 3 experimental data (crack widths of 2, 3, and 4 mm) are used for testing the performance of trained network.

3.4. Evaluation results

In order to illustrate the influence of feature selection on the prediction accuracy of defect width, the average prediction errors using only time domain features and frequency domain features, are compared with the prediction error using the combination of time and frequency domain features. The comparison is shown in Table 3 and it demonstrates that the GA-BPNN model trained with the combination of time and frequency features has the minimum average error of 2.15%, which is substantially smaller than the errors obtained from the model trained with only time-domain features and frequency-domain features, with the average relative error of 4.43% and 21.81%, respectively. It therefore concludes that it is more reliable to select the combination features for predicting the defect width using GA-BPNN model.

Fig. 7 shows the training performance of the GA-BPNN model using 5 features (time and frequency domain). It shows that all the data following the linear slope of 1, which indicates that there is no significant overfitting from the training, validation and testing of the GA-BPNN model, suggesting the performance of the model is stable and well. Based on the well-trained GA-BPNN model, the remaining 16 testing data including 13 simulation data and 3 experimental data is applied for evaluating the prediction performance of the network.

Fig. 8(a) shows that the predicted results including 13 simulation data and 3 experimental data are well located along the straight line with the slope of 1, indicating that the predicted crack widths are approximately the same as the actual value for both simulated and experimental signals. Fig. 8(b) shows the relative errors of the predicted defect widths that are all below 6% and the average error is 2.15%. Such low errors suggest that the combination of GA-BPNN model and numerical simulation is a cogent tool for evaluating the width of subsurface defects using laser ultrasonic technique.

4. Conclusion

In this work, an effective nondestructive evaluation method that enables the quantification of subsurface defects of metallic structure is proposed by the combination of an improved genetic algorithm-back propagation neural network (GA-BPNN) model and non-contact laser ultrasonic technique. An experimentally validated numerical model is firstly established to simulate the interaction of laser-generated Rayleigh ultrasonic waves with subsurface defects, which is subsequently utilized to generate a large number of labeled laser ultrasonic signals for training the GA-BPNN model. Five sensitive features including three time-domain features (maximum, minimum and peak-to-peak value of the Rayleigh ultrasonic waves) and two frequency-domain features (F_c, BW_{-6dB}) from 173 simulated signals are extracted for training the GA-BPNN model, and 13 simulated signals and 3 experimental signals are utilized as testing set to verify the performance of the trained GA-BPNN model. The GA-BPNN model trained with the combination of time and frequency features has the average error of 2.15%, which is substantially smaller than the errors obtained from the time-domain features and frequency-domain features, with average errors of 4.43% and 21.81%, respectively. This work proves the feasibility and reliability of the combination of GA-BPNN algorithm and numerical simulation to identify the width of subsurface defects using laser ultrasonic technique. In the future work, the developed method will be implemented for evaluating other damage cases, for instances, defect positions, defect heights and depths.

Credit author contribution statement

Kaixing Zhang: conceived the approach, evaluated the results and corrected the manuscript. **Gaolong Lv:** carried out the experiments and simulation, proposed the GA-BPNN algorithm, Writing - original draft. **Shifeng Guo:** Supervision, conceived the approach, evaluated the results and corrected the manuscript. **Dan Chen:** Formal analysis, proposed the GA-BPNN algorithm and corrected the manuscript. **Yanjun Liu:** guided the laser ultrasonic experiments and evaluated the results. **Wei Feng:** evaluated and commented on the results, Writing - original draft.

Declaration of competing interest

The authors declare that they have no known competing financial interests or personal relationships that could have appeared to influence the work reported in this paper.

Acknowledgments

The authors are grateful to the financial support from the National Natural Science Foundation of Guangdong (No.2016A030313177), Guangdong Frontier and Key Technological Innovation (No. 2017B090910013), the Science and Technology Innovation Commission of Shenzhen (No. ZDSYS20190902093209795, No. JCYJ20170818153048647 and No. JCYJ 20180507182239617), and the China Postdoctoral Science Foundation (No. 2020M672891).

Appendix A. Supplementary data

Supplementary data to this article can be found online at https://doi.org/10.1016/j.ndteint.2020.102339.

References

[1] Delrue S, Aleshin V, Sorensen M, De Lathauwer L. Simulation study of the localization of a near-surface crack using an air-coupled ultrasonic sensor array. Sensors 2017;17:930.
[2] Goueygou M, Abraham O, Lataste JF. A comparative study of two non-destructive testing methods to assess near-surface mechanical damage in concrete structures. Ndt & E International. 2008;41:448–56.
[3] Wang K, Fan Z, Su Z. Orienting fatigue cracks using contact acoustic nonlinearity in scattered plate waves. Smart Mater Struct 2018;27:09LT1.
[4] Guo S, Zhang L, Chen S, Tan CKI, Yao K. Ultrasonic transducers from thermal sprayed lead-free piezoelectric ceramic coatings for in-situ structural monitoring for pipelines. Smart Mater Struct 2019;28:075031.
[5] Guo S, Chen S, Zhang L, Liew WH, Yao K. Direct-write piezoelectric ultrasonic transducers for pipe structural health monitoring. Ndt & E International. 2019;107:102131.
[6] Tarraf J, Mustapha S, Fakih MA, Harb M, Wang H, Ayoub G, et al. Application of ultrasonic waves towards the inspection of similar and dissimilar friction stir welded joints. J Mater Process Technol 2018;255:570–83.
[7] Fakih MA, Mustapha S, Tarraf J, Ayoub G, Hamade R. Detection and assessment of flaws in friction stir welded joints using ultrasonic guided waves: experimental and finite element analysis. Mech Syst Signal Process 2018;101:516–34.
[8] Li H, Zhou Z. Numerical simulation and experimental study of fluid-solid coupling-based air-coupled ultrasonic detection of stomata defect of lithium-Ion battery. Sensors 2019;19:2391.
[9] Guo S, Zhang L, Mirshekarloo MS, Chen S, Chen YF, Wong ZZ, et al. Method and analysis for determining yielding of titanium alloy with nonlinear Rayleigh surface waves. Mater Sci Eng, A 2016;669:41–7.
[10] Chen D, Lv G, Guo S, Zuo R, Liu Y, Zhang K, et al. Subsurface defect detection using phase evolution of line laser-generated Rayleigh waves. Optic Laser Technol 2020;131:106410.
[11] Zhang K, Zhou Z. Quantitative characterization of disbonds in multilayered bonded composites using laser ultrasonic guided waves. Ndt & E International. 2018;97:42–50.
[12] Tian J, Dong X, Gao S, Yao Y. Multipoint fiber-optic laser-ultrasonic actuator based on fiber core-opened tapers. Optic Express 2017;25:29737–45.
[13] Montinaro N, Epasto G, Cerniglia D, Guglielmino E. Laser ultrasonics inspection for defect evaluation on train wheel. Ndt & E International. 2019;107:102145.
[14] Wang S, Echeverry J, Trevisi L, Prather K, Xiang L, Liu Y. Ultrahigh resolution pulsed laser-induced photoacoustic detection of multi-scale damage in CFRP composites. Appl Sci 2020;10:2106.
[15] Chang Y, Yang D, Guo Y. Laser ultrasonic damage detection in coating-substrate structure via Pearson correlation coefficient. Surf Coating Technol 2018;353:339–45.
[16] Liu P, Jang J, Yang S, Sohn H. Fatigue crack detection using dual laser induced nonlinear ultrasonic modulation. Optic Laser Eng 2018;110:420–30.
[17] Hernandez-Valle F, Dutton B, Edwards RS. Laser ultrasonic characterisation of branched surface-breaking defects. Ndt & E International. 2014;68:113–9.
[18] Guo H, Zheng B, Liu H. Numerical simulation and experimental research on interaction of micro-defects and laser ultrasonic signal. Optic Laser Technol 2017;96:58–64.
[19] Sun W, Ye M, Xu Y. Study of carbon dioxide emissions prediction in Hebei province, China using a BPNN based on GA. J Renew Sustain Energy 2016;8:043101.
[20] Srivastava S, Sadistap S. Data processing approaches and strategies for non-destructive fruits quality inspection and authentication: a review. Journal of Food Measurement and Characterization 2018;12:2758–94.
[21] Yang X, Chen S, Jin S, Chang W. Crack orientation and depth estimation in a low-pressure turbine disc using a phased array ultrasonic transducer and an artificial neural network. Sensors 2013;13:12375–91.
[22] Deng W, Ye B, Bao J, Huang G, Wu J. Classification and quantitative evaluation of eddy current based on Kernel-PCA and ELM for defects in metal component. Metals 2019;9:155.
[23] Kesharaju M, Nagarajah R, Zhang T, Crouch I. Ultrasonic sensor based defect detection and characterisation of ceramics. Ultrasonics 2014;54:312–7.
[24] Chen H, Liu H, Wang X, Bai Y. Defect detection research of laser ultrasonic based on the improved BP network. Recent Advances on Applied Mathematics and Computational Methods in Engineering 2015:102.
[25] Bagheri A, Pistone E, Rizzo P. Outlier analysis and artificial neural network for the noncontact nondestructive evaluation of immersed plates. Res Nondestr Eval 2015;26:154–73.
[26] Chen Y, Chen B, Yao Y, Tan C, Feng J. A spectroscopic method based on support vector machine and artificial neural network for fiber laser welding defects detection and classification. Ndt & E International. 2019;108:102176.
[27] Li K, Ma Z, Fu P, Krishnaswamy S. Quantitative evaluation of surface crack depth with a scanning laser source based on particle swarm optimization-neural network. Ndt & E International. 2018;98:208–14.
[28] Zhang K, Zhou Z, Zhou J, Sun G. Characteristics of laser ultrasound interaction with multi-layered dissimilar metals adhesive interface by numerical simulation. Appl Surf Sci 2015;353:284–90.
[29] Zhang K, Li S, Zhou Z. Detection of disbonds in multi-layer bonded structures using the laser ultrasonic pulse-echo mode. Ultrasonics 2019;94:411–8.
[30] Chen G, Fu K, Liang Z, Sema T, Li C, Tontiwachwuthikul P, et al. The genetic algorithm based back propagation neural network for MMP prediction in CO2-EOR process. Fuel 2014;126:202–12.
[31] Zhou Y-t, Xia Y-f, Jiang L, Long S, Yang D. Modeling of the hot flow behaviors for Ti-6Al-4V-0.1 Ru alloy by GA-BPNN model and its application. High Temp Mater Process 2018;37:551–62.
[32] Ren C, An N, Wang J, Li L, Hu B, Shang D. Optimal parameters selection for BP neural network based on particle swarm optimization: a case study of wind speed forecasting. Knowl Base Syst 2014;56:226–39.
[33] Cai Y, Zheng W, Zhang X, Zhangzhong L, Xue X. Research on soil moisture prediction model based on deep learning. PloS One 2019;14:e0214508.
[34] Li H, Wang J, Lu H, Guo Z. Research and application of a combined model based on variable weight for short term wind speed forecasting. Renew Energy 2018;116:669–84.
[35] Yan F, Lin Z. New strategy for anchorage reliability assessment of GFRP bars to concrete using hybrid artificial neural network with genetic algorithm. Compos B Eng 2016;92:420–33.
[36] Zhang F, Mukhtar YMF, Liu B, Li J. Application of ANN to predict the apparent viscosity of waxy crude oil. Fuel 2019;254:115669.
[37] Oreski S, Oreski G. Genetic algorithm-based heuristic for feature selection in credit risk assessment. Expert Syst Appl 2014;41:2052–64.
[38] Tompkins G, Azadivar P. Genetic algorithms in optimizing simulated systems. Winter Simulation Conference Proceedings 1995:757–62. IEEE; 1995.
[39] Elattar EE. A hybrid genetic algorithm and bacterial foraging approach for dynamic economic dispatch problem. Int J Electr Power Energy Syst 2015;69:18–26.
[40] Hu Y, Li J, Hong M, Ren J, Lin R, Liu Y, et al. Short term electric load forecasting model and its verification for process industrial enterprises based on hybrid GA-PSO-BPNN algorithm—a case study of papermaking process. Energy 2019;170:1215–27.
[41] Wang L, Zeng Y, Chen T. Back propagation neural network with adaptive differential evolution algorithm for time series forecasting. Expert Syst Appl 2015;42:855–63.
[42] Gou J, Fan Z-W, Wang C, Guo W-P, Lai X-M, Chen M-Z. A minimum-of-maximum relative error support vector machine for simultaneous reverse prediction of concrete components. Comput Struct 2016;172:59–70.
[43] Kisi O, Shiri J, Tombul M. Modeling rainfall-runoff process using soft computing techniques. Comput Geosci 2013;51:108–17.
[44] Chandwani V, Agrawal V, Nagar R. Modeling slump of ready mix concrete using genetic algorithms assisted training of Artificial Neural Networks. Expert Syst Appl 2015;42:885–93.
[45] Kusumo F, Silitonga AS, Masjuki HH, Ong HC, Siswantoro J, Mahlia TMI. Optimization of transesterification process for Ceiba pentandra oil: a comparative study between kernel-based extreme learning machine and artificial neural networks. Energy 2017;134:24–34.